

## ON THE ORIGIN OF THE ORION AND MONOCEROS MOLECULAR CLOUD COMPLEXES

J. FRANCO,<sup>1,2</sup> G. TENORIO-TAGLE,<sup>1,2</sup> P. BODENHEIMER,<sup>2,3</sup> M. RÓŻYCZKA,<sup>2,4</sup> AND I. F. MIRABEL<sup>5</sup>

Received 1988 January 4; accepted 1988 April 12

### ABSTRACT

A model for the origin of the Orion and Monoceros molecular cloud complexes, which are located more than 100 pc away from the galactic plane, is presented. The model is based on two-dimensional hydrodynamic simulations for the interaction of high-velocity clouds and the disk of the Galaxy. Cloud-galaxy collisions are able to generate massive shocked layers and self-gravity can then provide the conditions for the transformation of these layers into molecular clouds. The clouds formed by this process maintain the motion of their parental shocked gas and reach positions located far away from the plane. The location and mass observed in the Orion and Monoceros molecular complexes can be explained by a collision of a high-velocity cloud with the galactic gaseous disk in the solar neighborhood. According to this model both complexes were formed some  $6 \times 10^7$  yr ago, when the original shocked layer was fragmented by galactic tidal forces.

*Subject headings:* hydrodynamics — interstellar: molecules

### I. INTRODUCTION

The Orion and Monoceros molecular cloud complexes are large cloud systems located almost in the same direction in the sky and each containing some  $2 \times 10^5 M_{\odot}$  in molecular gas (see Maddalena *et al.* 1986 and references therein). Aside from this similarity in their mass content, the main bodies of both complexes (the Orion A and Mon R2 clouds) are situated more than 100 pc below the galactic plane and it has been suggested that they may even be physically connected (Thaddeus 1982; Maddalena *et al.* 1986). Their heights are certainly peculiar for such giant molecular clouds (GMCs): the scale height of molecular gas in the solar neighborhood is only 75 pc and even the less massive diffuse H I clouds have a scale height slightly smaller than 100 pc (Sanders, Solomon, and Scoville 1984). Thus, Orion and Monoceros are either located outside the main H I disk or, at their location, the disk itself has been heavily distorted by a strong perturbation. Either alternative requires a large amount of energy and momentum in order to accelerate the interstellar gas out of the galactic plane.

The required energy and momentum could be obtained from stellar winds and supernovae in OB associations or from collisions of high-velocity H I clouds (HVCs) with the galactic disk. However, star-driven bubbles seem unsuitable to explain the observed asymmetries of the region. Orion has no counterparts at the other side of the plane and there are no stellar groups or gaseous features at the locations expected in a shell driven by stellar winds. On the other hand, HVC-galaxy interactions provide an appealing scheme to explain the properties of these two complexes (Franco 1986). The basic idea is simple: the shock produced by a HVC-galaxy collision collects and accelerates the interstellar gas, and the resultant structures evolve in the direction of motion of the impinging cloud. Recent hydrodynamical simulations show that these events are certainly able to distort the gaseous disk and can generate large-scale

and massive interstellar structures (Tenorio-Tagle *et al.* 1986, 1987; hereafter Paper I and Paper II).

Here we present a detailed model for the origin of the Orion and Monoceros cloud complexes and show that a single HVC-galaxy collision can explain their main observed features. Section II is devoted to a review of the observed properties of the region. A general model for GMC formation by HVC-galaxy interactions is presented in § III. The case of the Orion-Monoceros complexes is analyzed in § IV, and a brief discussion is given in § V.

### II. PROPERTIES OF THE REGION

#### a) Orion and Monoceros

The Orion and Monoceros cloud complexes are massive and filamentary GMCs situated in the third galactic quadrant, in the direction of the Gould belt, and at distances of about 500 and 850 pc from the Sun, respectively. Their mass is distributed in a network of clouds with a complicated morphology (Fig. 1). Their main components, the Orion A and Mon R2 clouds, contain a sizeable fraction of the molecular gas ( $\sim 10^5 M_{\odot}$  each) and seem to share some interesting similarities (see Maddalena *et al.* 1986, and references therein): (i) both clouds are located some 150 pc below the  $b = 0^{\circ}$  plane, (ii) they are elongated almost parallel to the galactic plane and have linear extents close to 100 pc, and (iii) both clouds have an overall velocity gradient which may be indicative of retrograde rotation with an angular speed  $\omega \sim (1-3) \times 10^{-15} \text{ s}^{-1}$ . These similarities, despite the fact that they are separated by  $\sim 400$  pc, could be suggestive of a common origin.

The Monoceros complex exhibits several tracers of recent star formation (i.e., embedded infrared sources, compact H II regions, etc.; see review by Maddalena *et al.* 1986), and the data on Mon R2 indicate that the star-forming activity started some  $10^7$  yr ago (Hughes and Baines 1985), which could be used as a rough lower limit to the age of the molecular complex. On the other hand, Orion has well-studied OB subgroups and a large number of low-mass stars. The oldest OB subgroup, Ori Ia, has an estimated age of  $1.2 \times 10^7$  yr (Blaauw 1964), and the low-mass star data suggest an age spread of at least  $3 \times 10^7$  yr (Isobe 1982, 1987). Hence, the age of the Orion complex seems to be greater than  $\sim 3 \times 10^7$  yr.

<sup>1</sup> Instituto de Astronomía-UNAM, Mexico.

<sup>2</sup> Max-Planck-Institut für Physik und Astrophysik.

<sup>3</sup> Lick Observatory, Board of Studies in Astronomy and Astrophysics, University of California, Santa Cruz.

<sup>4</sup> Warsaw University Observatory.

<sup>5</sup> Instituto de Astronomía y Física del Espacio, Buenos Aires.

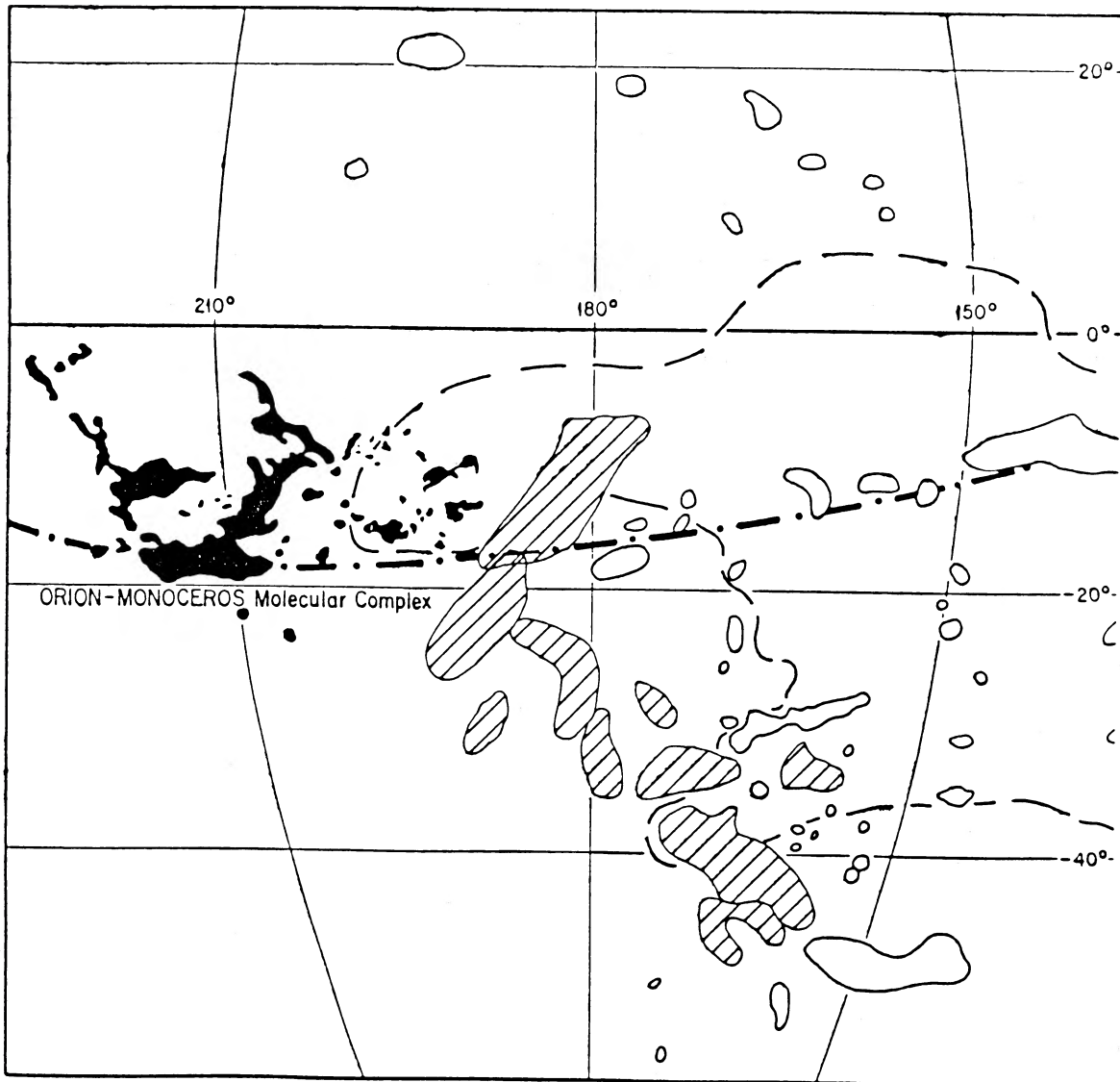


FIG. 1.—Map of the Orion-Monoceros region. The Orion and Monoceros cloud complexes, which are the only CO features considered in the figure, are shown as black filled structures (adapted from Maddalena *et al.* 1986). H I high-velocity clouds with  $V_{\text{LSR}} \leq -150 \text{ km s}^{-1}$  are filled with diagonal lines, and HVCs with  $-80 \text{ km s}^{-1} \geq V_{\text{LSR}} \geq -150 \text{ km s}^{-1}$  are delineated by thin solid lines (adapted from Mirabel 1981*a*). The thin dashed line shows the boundaries of the anticenter shell (from Heiles 1984). The thick dot-dashed line shows the approximate location of the Gould belt (from Stothers and Frogel 1974).

The region has several H $\alpha$  and 21 cm features that extend even farther away from the galactic plane (Heiles and Jenkins 1976; Reynolds and Ogden 1979 and references therein). These H I and H $\alpha$  structures seem to have comparable amounts of matter, and their origin has been ascribed to the activity of the massive stars in Orion. The mass in the 21 cm emitting gas is probably close to  $\sim 2 \times 10^5 M_{\odot}$  (Maddalena *et al.* 1986), which implies a total gaseous mass of  $\sim 9 \times 10^5 M_{\odot}$  for the whole Orion-Monoceros region. The total mass in stars is difficult to derive, but a rough extrapolation of the number of observed stars in the Orion Nebula suggests that the stellar content can be as high as  $\sim 10^5 M_{\odot}$  (Isobe 1987).

#### b) The Gould Belt

The Gould belt is a ring of relatively young stars and interstellar clouds surrounding the Sun and extending up to 500 pc in radius (Lesh 1968; Stothers and Frogel 1974; Frogel and

Stothers 1977; Taylor, Dickman, and Scoville 1987). It is inclined some  $12^{\circ}$  to  $18^{\circ}$  (see Fig. 1) with respect to the galactic plane and both the gas and the stars have expansion velocities of about  $5 \text{ km s}^{-1}$ . The age of the belt, estimated from different types of studies, is in the range  $3 \times 10^7$ – $9 \times 10^7$  yr with a likely value around  $6 \times 10^7$  yr.

The origin of this inclined and expanding structure may not be due to a single event. Its expansion can be understood in terms of a model with a high pressure disturbance in the plane, supposedly an OB association, that was originally located  $\sim 170$  pc away from the Sun in the direction  $130^{\circ}$  (Olano 1982). The inclination to the plane and the distribution of molecular clouds, however, cannot be explained by such a simple expansion model (see Taylor, Dickman, and Scoville 1987). Actually, the stellar vertical motions in the belt indicate that the tilt is related to an oscillatory motion, which can be interpreted as if  $\sim 6 \times 10^7$  yr ago a part of the solar neighbor-

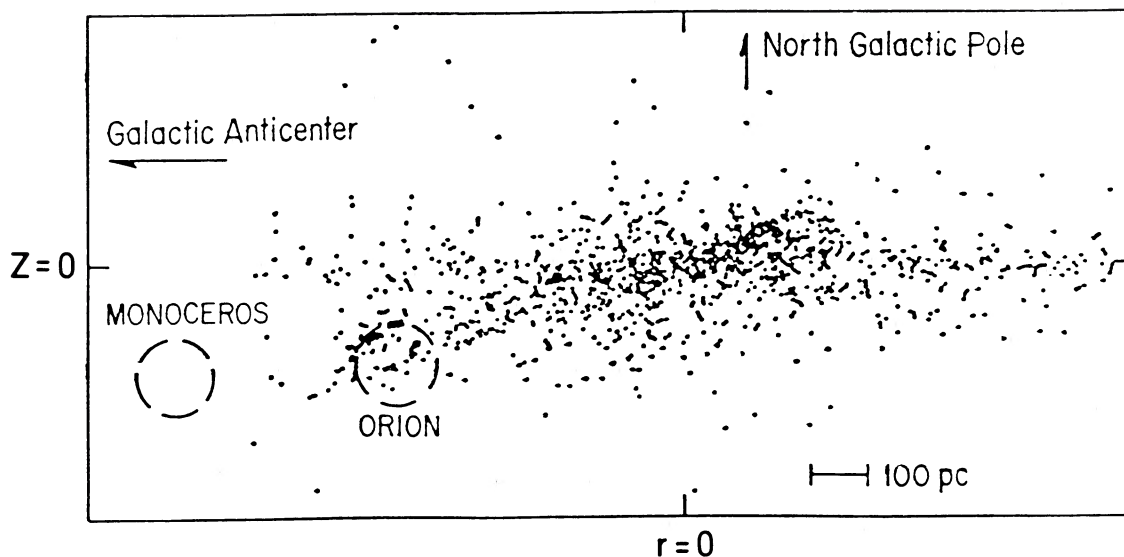


FIG. 2.—Projected positions of O-B stars within 800 pc from the Sun, which is located at  $r = z = 0$  (adapted from Stohers and Frogel 1974). The approximate projections of the main bodies of Orion and Monoceros are also indicated.

hood was “knocked out of the galactic plane” by some energetic disturbance (Frogel and Stohers 1977).

Figure 2 shows the projected positions of O-B stars within 800 pc from the Sun on a plane perpendicular to the galactic plane. The extent and inclination of the Gould belt are clearly apparent in the figure. The Orion A cloud lies near its outer boundaries in the southernmost tip but the distance to Monoceros,  $\sim 850$  pc, rules out any physical connection between Mon R2 and the belt.

#### c) Other Peculiarities of the Molecular Gas in the Galaxy

The distribution of molecular gas in the inner Galaxy has a slowly varying scale height and displays some distortions from the  $b = 0^\circ$  line (Sanders, Solomon, and Scoville 1984). The scale height increases from about 50 pc at  $R \sim 5$  kpc to 75 pc at the solar neighborhood, whereas the main molecular concentrations (the mean  $H_2$  “plane”) in the first quadrant tend to be displaced below the  $b = 0^\circ$  plane (reaching heights of  $z = -40$  pc at  $R \sim 5$  kpc) and some of these vertical displacements are indicative of oscillations or distortions with amplitude similar to the scale height. In addition, a recent CO study has revealed the existence of a massive cloud ( $\sim 10^5 M_\odot$ ) located some  $\sim 200$  pc away from the plane in the direction of Lupus (Nyman *et al.* 1987). Together with Orion and Monoceros, these oscillations and the location of the recently discovered GMC show that large  $z$ -excursions of the gas could be usual features in the disk and suggest the continuous action of strong perturbations.

The velocity dispersion among molecular clouds in the inner Galaxy is fairly constant between 3 to 8  $\text{km s}^{-1}$ , and there also exist large-scale streaming motions with 5 to 15  $\text{km s}^{-1}$  (Clemens 1985; Stark and Brand 1988). The large-scale streams are usually ascribed to spiral arms or large mass concentrations, and it is unclear if they are related to the observed vertical displacements. In any case, the constancy in the cloud-cloud dispersions indicates that these two types of motions are not strongly coupled or that the perturbations induced by the large-scale streams are short-lived. This point is reinforced by a recent study of Avedisova and Palouš (1988),

which found a constant velocity dispersion among star forming regions of about 6  $\text{km s}^{-1}$ .

#### d) High-Velocity Clouds

The region contains a large number of HVCs with a wide range of velocities (see Fig. 1), but their distances are unknown and it is difficult to derive their mass and sizes (cf. Mirabel 1981a). The ones with the more negative velocities seem to be part of the Magellanic Stream and are known as the “anticenter complex.” Mirabel (1982) has found evidence for a possible interaction between one of these clouds and the gaseous disk, and he estimates that the total energy injected in the collision can be larger than  $5 \times 10^{51}$  ergs.

There is also a large ( $\sim 30^\circ$  in size) and nearly complete H I shell, the anticenter shell, centered near  $l = 180^\circ$  and with velocities as high as  $V_{\text{LSR}} = -90$   $\text{km s}^{-1}$  (Heiles 1984). Its origin is uncertain, but Kulkarni and Mathieu (1986) suggest that it is the result of a HVC-galaxy interaction. Their distance estimates, based in the spectra of 17 stars, indicate that the anticenter shell is more distant than 500 pc.

Additional evidence for possible HVC-galaxy collisions has been found in the direction of the Draco nebula (Kalberla, Herbstmeier, and Mebold 1984; Hirth, Mebold, and Müller 1985) and in the spiral galaxy M101 (van der Hulst and Sancisi 1988). In the case of the Draco nebula the interaction is associated with a molecular cloud, but in M101 the observations have been made only in the 21 cm line.

### III. FORMATION OF MOLECULAR CLOUDS BY HVC INTERACTIONS

The collisions between HVCs and the disk of our Galaxy represent a rich potential source of energy and momentum for the interstellar medium, and these interactions may be responsible for a variety of large-scale gaseous structures (Papers I and II). A collision generates a thin shocked layer which collects and accelerates galactic gas in the direction of motion of the HVC. The details of the interactions and the size of the perturbed regions, however, depend on the original cloud parameters: clouds with larger column densities penetrate deeper into the galaxy and larger clouds generate struc-

tures with larger lateral dimensions. The cloud geometry is also important in the postcollision evolution. Spherical clouds, with a peak in column density along the symmetry axis, generate "centrally condensed" shocked layers, and these central regions penetrate faster into the Galaxy than the rest of the layer. Flattened clouds, on the other hand, do not have such a preferential axis and the resulting shocked layers evolve in a more coherent manner (Paper II).

Here we are interested in collisions which can trigger the formation of molecular clouds. The chemistry behind shock fronts incident upon atomic hydrogen is dependent on the abundance of  $H_2$  formed in the compressed gas and on the dissociative UV radiation field (see review by McKee and Hollenbach 1980). For simplicity, it is assumed that the molecular species (i.e., CO,  $NH_3$ , etc.) are built up when the photodissociation rates inside the shocked layer are reduced by dust opacity and that condition is achieved in the solar neighborhood when the total shocked gas column density is  $N_t \geq 10^{21} \text{ cm}^{-2}$  (Franco and Cox 1986). Gas-phase chemical models indicate that the process takes several million years (cf. Gerola and Glassgold 1978; Tarafdar *et al.* 1985). Thus, within this simplified scheme, the transformation of the shocked layer into a molecular cloud simply requires the maintenance of the high-opacity column density over a time scale of the order of  $10^7$  yr.

a) *The Evolution of the Shocked Layer as It Falls toward the Galactic Plane*

This part of the problem is analyzed with the two-dimensional simulations for head-on collisions described in Paper II. The discussion is focused on models with uniform density cylindrical clouds, and approximate corrections for the spherical case are also indicated. Note that § 2.1 in Paper II describes a Gaussian density stratification for the gaseous disk, but the actual calculations were performed with an exponential density distribution. In this paper the gaseous disk in the solar neighborhood is actually represented by a single Gaussian density distribution in the  $z$ -direction

$$\rho_g(z) = \rho_g(0)e^{-z^2/H^2}, \quad (1)$$

with a midplane gas density  $\rho_g(0) = 5 \times 10^{-24} \text{ g cm}^{-3}$ , and an effective height  $h = \pi^{1/2} H/2 = 10^2 \text{ pc}$  (see Paper II). The sound speed in the disk is assumed to be equal to the cloud-cloud velocity dispersion among the "normal" population of diffuse H I clouds,  $c \sim 8 \text{ km s}^{-1}$  (cf. Kulkarni and Fich 1985), and the gravitational acceleration in the  $z$ -direction within 300 pc from midplane is approximated by  $g_z = -2 \times 10^{-9} Z_2 \text{ cm s}^{-2}$ , where  $Z_2$  is the height in units of  $10^2 \text{ pc}$  (Spitzer 1978). The resulting total interstellar pressure at midplane is  $p(0) = 1.7 \times 10^{-12} \text{ dyn cm}^{-2}$ , which is higher than the commonly used "nominal" pressure,  $\sim 4 \times 10^{13} \text{ dyn cm}^{-2}$ , but it is well within the local limits imposed by the soft X-ray diffuse background (Kraushaar 1979). The cooling function contains the cooling due to molecular hydrogen (see Paper II) but, due to heavy computational demands, no other molecular species are considered. Similarly, the code does not include self-gravity in the shocked layer nor the distortions produced by galactic rotation. These effects, however, become important in the late evolution of the shocked layer and they are considered in an approximate manner in the following subsections.

Figures 3a and 3b display the evolution of two numerical simulations. The clouds in these examples had the same original velocities,  $V_c = 100 \text{ km s}^{-1}$ , and dimensions, 100 pc in height and 200 pc in radius, but different densities:  $n_c = 0.3$

$\text{cm}^{-3}$  and  $n_c = 1 \text{ cm}^{-3}$ , respectively. The cloud centers were located 500 pc above midplane at the beginning of the runs.

The collision ends when the whole cloud has been shocked. The time scale for this phase,  $t_{\text{ref}}$ , depends on the ratio of cloud to ambient densities (Papers I and II) and, hence, on the chosen initial conditions. For the models considered here and in Paper II, with initial distances from the plane between 400 and 700 pc, the time for a cloud collision can be approximated by

$$t_{\text{ref}} \approx 3.5 V_c^{-1} D_c = 3.5 \times 10^6 V_2^{-1} D_2 \text{ yr}, \quad (2)$$

where  $V_2 = V_c/10^2 \text{ km s}^{-1}$ , and  $D_2$  is the HVC height in units of  $10^2 \text{ pc}$ . By this time, which is large compared to the cooling time, the shocked layer has cooled below  $10^4 \text{ K}$  and its column density and velocity are restricted to  $N_t(t_{\text{ref}}) \leq 3N_c/2$  (i.e., the swept-up column density is smaller than about half the original cloud column density,  $N_c = n_c D_c$ ) and  $V_t(t_{\text{ref}}) \geq 3V_c/2$ . The corresponding location of the shocked layer,  $z_{\text{ref}}$ , is independent of the initial conditions (for initial distances from the plane above 400 pc) and it is defined by

$$\text{erf}(z_{\text{ref}}/2^{1/2}H) = 1 - [2n_c/\pi n(0)]^{1/2} D_c/H, \quad (3)$$

where  $\text{erf}(x)$  is the error function, and  $n(0)$  is the disk volume density at midplane. The resulting values for Figures 3a and 3b are  $z_{\text{ref}} \sim 150 \text{ pc}$  and  $\sim 100 \text{ pc}$ , respectively. It is clear that impinging clouds with  $n_c^{1/2} D_c \geq [\pi n(0)/2]^{1/2} H$  can reach the galactic plane before they are completely shocked.

The subsequent evolution proceeds in the momentum-conserving stage and the shocked layer collects interstellar mass and generates a rear vacuum region, the rear cavity, as it penetrates supersonically into the disk. The collision also generates lateral shocks which induce the sideways growth of the perturbed region. These lateral shocks, however, decay faster than the one induced in the direction of motion of the original HVC, the main shock. The rest of the paper deals with the properties of the layer generated by this main shock, simply referred to as the remnant, whose radius remains roughly equal to that of the original cloud over most of the evolution.

The pressure difference between the remnant and the rear cavity promotes the expansion of the shocked gas. The effects of this expansion depend on the ratio of the remnant velocity,  $V_r$ , to the sound speed in the postshock relaxation layer (i.e., if the sound crossing time inside the remnant is larger than the crossing time of the remnant through the half disk, the shocked gas has no time to expand back into the cavity). The numerical simulations (Figs. 3; Paper II) show that the remnant suffers a significant broadening before reaching the galactic plane, and some mass is lost as the layer expands into the rear cavity, if the original cloud momentum per unit area is

$$\mu N_c V_c \leq 3c \int_0^\infty \rho(z) dz,$$

where  $\mu$  is the mass per particle. For the solar neighborhood this is equivalent to a HVC column density below the critical value

$$N_{\text{crit}} \approx 1.5 \times 10^{20} V_2^{-1} \text{ cm}^{-2}. \quad (4)$$

The value of this constraint is dependent on the cloud geometry and the corresponding value for spherical clouds is  $\sim 2$  times higher.

In the collision displayed in Figure 3a the cloud column density is below the critical value, and the shocked layer expansion into the rear cavity is clearly apparent in the frames.

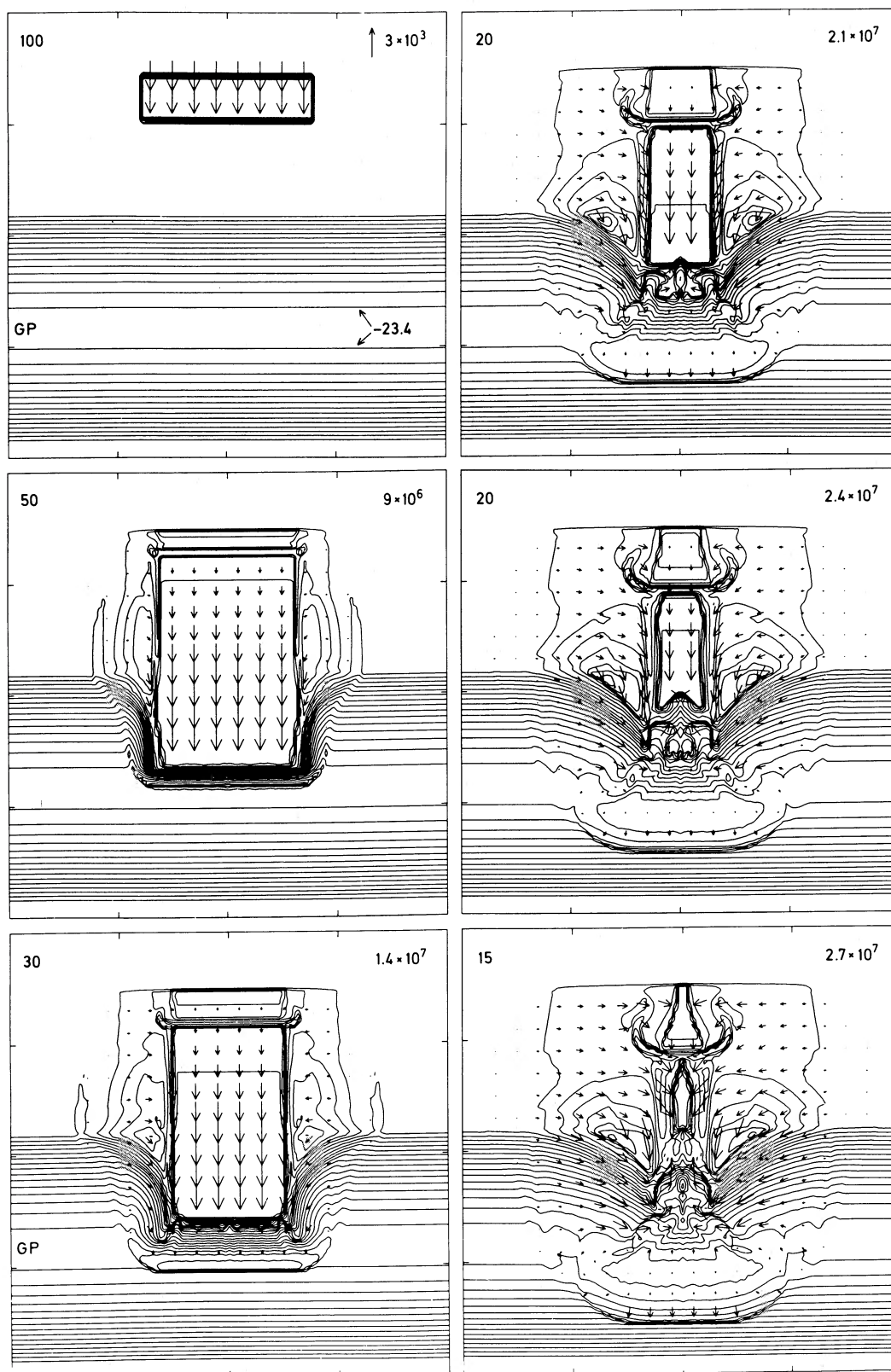


FIG. 3a

FIG. 3.—(a) Evolution of the collision of a cylindrical HVC with  $n_c = 0.3 \text{ cm}^{-3}$ ,  $V_c = 100 \text{ km s}^{-1}$ ,  $r_c = 200 \text{ pc}$ , and  $100 \text{ pc}$  in height. The frames show isodensity contours with  $\Delta \log \rho = 0.2$ . The maximum contour level in  $\log \rho$  is indicated in the first frame. The distance between marks in the frames is  $250 \text{ pc}$ . The length of the standard velocity vector (in  $\text{km s}^{-1}$ ) and the evolutionary time scales (in yr) are shown in the left and right upper corners, respectively. (b) Same as in Fig. 3(a), except that  $n_c = 1 \text{ cm}^{-3}$ .

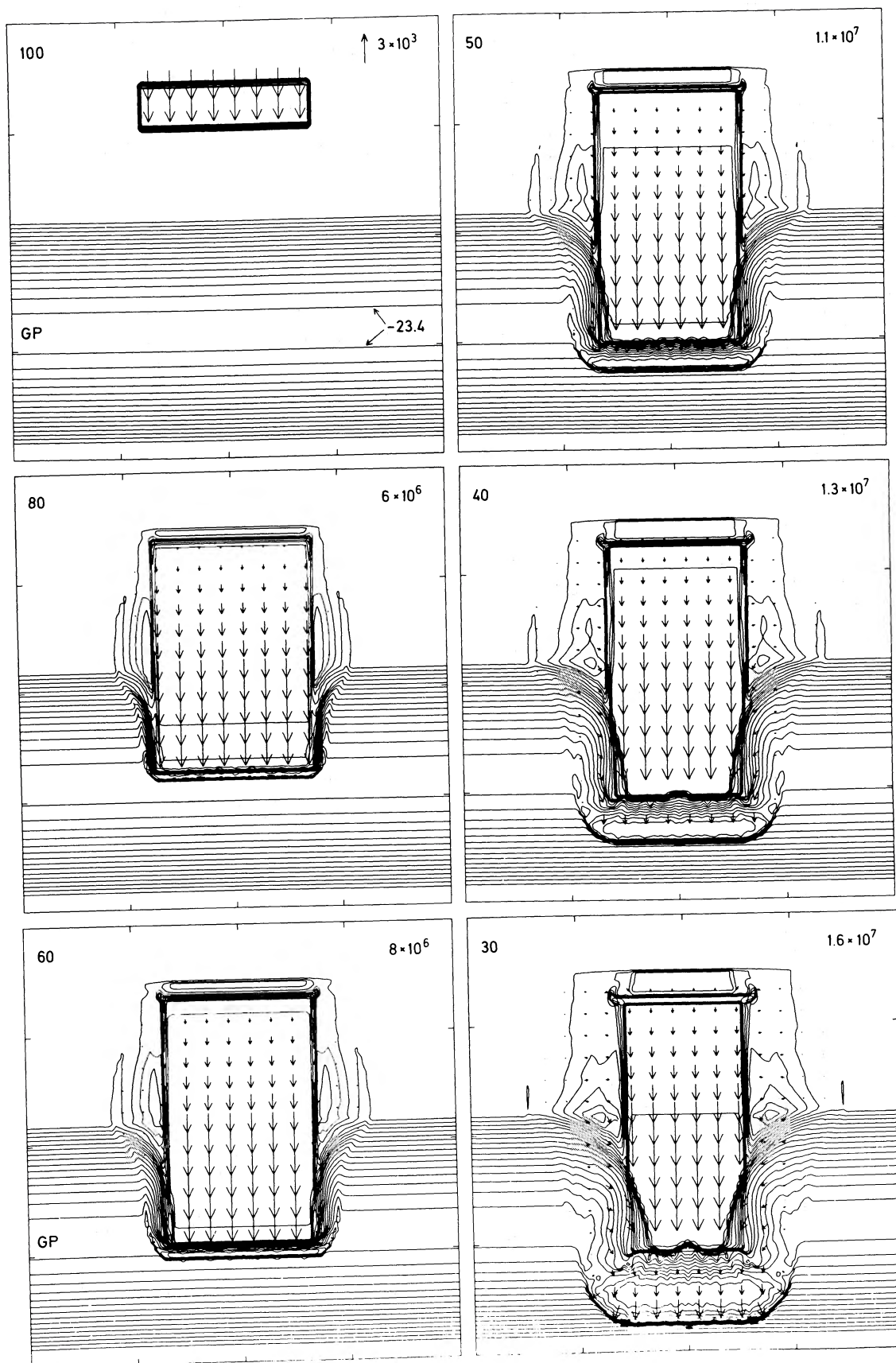


FIG. 3b  
831

In contrast, the cloud column density in Figure 3*b* is above  $N_{\text{crit}}$  and the remnant reaches the galactic plane with almost no broadening. The difference is noteworthy and the likelihood of GMC formation by HVC-galaxy interactions is certainly dependent on this effect. The reduction of the molecular photo-dissociation rates in the remnant interior requires a total column densities above  $10^{21} \text{ cm}^{-2}$  (Franco and Cox 1986), and this high-opacity criterion is never fulfilled when  $N_c < N_{\text{crit}}$ . Such a restriction confines the molecular cloud progenitors to colliding HVCs with  $N_c > N_{\text{crit}}$ , and the rest of the paper is focused on these collisions. The case shown in Figure 3*b* is an illustrative example of these type of events.

The resulting remnants sink into the disk without mass-loss effects (except for spherical clouds where some mass is lost near the remnant edges) and their column densities, masses, and velocities before reaching the plane can be approximated by

$$N_l(t) = N_c + N_g(t), \quad (5a)$$

$$M_l(t) = \pi r_c^2 \mu N_l(t), \quad (5b)$$

$$V_l(t) = [1 + N_g(t)/N_c]^{-1} V_c, \quad (5c)$$

with the swept-up column density

$$N_g(t) = N_{1/2} \{1 - \text{erf}[z(t)/H]\}, \quad (5d)$$

where  $N_{1/2} = 6 \times 10^{20} \text{ cm}^{-2}$  is the gas column density of the half disk,  $r_c$  is the colliding cloud radius (for spherical clouds the remnant radius should be reduced to  $\sim 2r_c/3$ ), and  $z(t)$  is the height of the main shock at time  $t$ .

The time at which the plane is reached is referred to as  $t_{\text{GP}}$  and the corresponding values in equations (5) are denoted by  $N_0$ ,  $M_0$ , and  $V_0$ . This time scale is also dependent on the chosen initial position of the cloud above the plane, but the time difference  $t_{\text{GP}} - t_{\text{ref}}$  is not. Integration of equation (5c) gives the appropriate evolution after  $t_{\text{ref}}$  and one obtains

$$t_{\text{GP}} - t_{\text{ref}} = 10^6 V_2^{-1} [2N_{1/2}/\pi N_c + z_{\text{ref}}/h] \text{ yr}. \quad (6)$$

These time scales, which are typically smaller than  $10^7$  yr (about  $2 \times 10^6$  yr for the case shown in Fig. 3*b*), indicate that galactic tidal effects can be neglected in the evolution before  $t_{\text{GP}}$ , but they may become important at later times (see § IIIb). Also notice that remnants generated by HVC with  $N_c > 4 \times 10^{20} \text{ cm}^{-2}$  can begin their transformation into a molecular cloud before crossing the galactic plane.

#### b) Evolution after Passage through the Plane

The gravitational field and the ambient density gradient reverse after the remnant crosses the galactic plane. The combined action of these two changes, along with the pressure difference between the remnant and the rear cavity, stretch the remnant in the  $z$ -direction and they can lead to its final disruption: the gravitational field pulls the remnant back toward the plane while the main shock speeds up as it encounters a negative density gradient. As the remnant expands its internal pressure,  $P$ , drops down and the shock strength weakens unless the remnant is held together by self-gravitational forces. If self-gravity remains negligible, the expansion continues until the remnant reaches pressure equilibrium with its surroundings and the shocked gas merges with the ambient medium. Otherwise, if self-gravity becomes dominant, the expansion and pressure falloff are halted as the remnant adjusts into a centrally condensed structure and the shocked gas is maintained as a dense cloud with a large column density. The resulting opaque

structure evolves as a single entity and can become a molecular cloud.

#### i) Self-Gravity

The cylindrical remnant, with radius  $r_c$  and total height  $2w$ , can be approximated (see Fig. 3) by an oblate spheroid with eccentricity

$$\epsilon = (1 - w^2/r_c^2)^{1/2},$$

and internal pressure

$$P = \mu n(z) V_l^2 \approx \frac{N_l k T}{2w} = \frac{N_l k T}{2r_c (1 - \epsilon^2)^{1/2}}, \quad (7)$$

where  $n(z)$  is the disk density distribution,  $k$  is the Boltzmann constant, and  $T$  is the temperature in the center of the remnant. For the velocities and column densities involved the temperature in the postshock relaxation layer is always below  $2 \times 10^3$  K, and a reference value of  $10^3$  K can be used as a rough estimator in order of magnitude computations. The self-gravitational acceleration at the remnant boundaries are (Mestel 1965)

$$\ddot{r}_c = -\pi G \mu N_l f(\epsilon) = -\frac{GM_l}{r_c^2} f(\epsilon), \quad (8a)$$

and

$$\ddot{w} = -2\pi G \mu N_l g(\epsilon), \quad (8b)$$

where  $G$  is the gravitational constant and

$$f(\epsilon) = \epsilon^{-3} [\sin^{-1} \epsilon - \epsilon(1 - \epsilon^2)^{1/2}], \quad (9a)$$

$$g(\epsilon) = \epsilon^{-3} [\epsilon - (1 - \epsilon^2)^{1/2} \sin^{-1} \epsilon]. \quad (9b)$$

These functions are slowly varying and have a narrow range of values. For small eccentricities (i.e.,  $\epsilon \leq 0.1$ )  $f(\epsilon) \approx 0.67$  and  $g(\epsilon) \approx 0.33$ , whereas for  $0.75 \leq \epsilon \leq 1$  (i.e.,  $w \leq 0.66r_c$ )  $f(\epsilon)$  varies from 0.83 to  $\pi/2$  and  $g(\epsilon)$  from 0.45 to 1.

Self-gravity in the  $z$ -direction is achieved when the column density is

$$N_{\text{SG}} \approx \left[ \frac{2P}{\mu^2 \pi G g(\epsilon)} \right]^{1/2} = 2.4 \times 10^{21} [e^{z^2/H^2} g(\epsilon)]^{-1/2} \frac{V_l}{c} \text{ cm}^{-2}, \quad (10)$$

or, using equation (7),

$$N_{\text{SG}} \approx \frac{kT}{\mu^2 \pi G r_c (1 - \epsilon^2)^{1/2} g(\epsilon)} = 4 \times 10^{20} \frac{T_3}{r_2 (1 - \epsilon^2)^{1/2} g(\epsilon)} \text{ cm}^{-2}, \quad (11)$$

where  $T_3 = T/10^3$  K, and  $r_2 = r_c/10^2$  pc. The required column density could be lowered by a small amount if one assumes a plane-parallel shock (Elmegreen and Elmegreen 1978), but the final results of our model are insensitive to these small changes.

The eccentricity decreases as the remnant expands but the function  $(1 - \epsilon^2)^{1/2} g(\epsilon)$  remains nearly constant, at about  $\sim 0.3$ , for  $0 \leq \epsilon \leq 0.8$ . Thus, using equation (11) self-gravity is eccentricity independent for  $\epsilon$  below 0.8 and the minimum column density,  $N_{\text{min}}$ , below which no self-gravitating stage can be reached is given by

$$N_{\text{min}} \approx 1.2 \times 10^{21} T_3 r_2^{-1} \text{ cm}^{-2}. \quad (12a)$$

However, if  $N_{\min}$  is reached but the eccentricity is larger than 0.8 the cloud is not yet self-gravitating. Assuming  $\epsilon = 0.8$ , the minimum distance from the plane at which the self-gravitating stage can be achieved is defined by

$$z \approx H[2 \ln(3r_2/2T_3)]^{1/2}. \quad (12b)$$

Equation (12a) imposes a severe restriction on the molecular cloud progenitors because remnants with  $r_2 \leq 0.5$  require unrealistically large column density values in order to survive the passage of the plane. Hence, only impinging clouds with radius larger than about 50 pc are suitable as progenitors of molecular clouds and, given the large dimensions involved, the resulting clouds are large and massive (i.e., GMCs).

In the case of Figure 3b the minimum column density is about  $10^{21} \text{ cm}^{-2}$ , which is coincidental with the high-opacity criterion, and it is reached at about 50 pc after passage through the plane. The self-gravitating stage, however, is achieved at a later time when the remnant has moved  $\sim 150$  pc from the galactic plane (eq. [12b]) and it has already collected an even larger column density. This occurs some  $10^7$  yr after passage through the plane. Thus, the transformation of this remnant into a molecular cloud is warranted by the maintainance of the high-opacity column density over the appropriate time scale.

The expansion of the shocked gas is clearly apparent in Figure 3b but the simulations do not include the action of self-gravity, and the layer relaxation into the self-gravitating stage cannot be resolved. These numerical simulations, however, give a fair description of the remnant evolution up to the early phases of the self-gravitational stage and the last frame in Figure 3b, computed at  $\sim 10^7$  yr after passage through the plane, shows the approximate time when self-gravity is expected to set in. The evolution of this coherent structure is simply described by the motion of the center of mass, which is discussed in the following subsection.

#### ii) Motion of the Self-gravitating Remnant

The equation of motion for the center of mass of the remnant is

$$\ddot{z} = g_z - \frac{n(z)}{N_l} V_l^2 = -\alpha z - \beta e^{-z^2/H^2} z^2, \quad (13)$$

where  $g_z = -\alpha z$  is the gravitational acceleration of the disk, and  $\beta = n(0)/N_l$ . The second term in the right-hand side represents the deceleration due to the mass growth in the supersonic case, or, the interstellar drag term in the subsonic case. The pressure and the column density vary as the collision proceeds and the shock description is time-dependent. Nevertheless, the evolution can be approximated without solving exactly the mass growth term because the values of  $\beta$  are simply bounded by

$$\beta_{\max} = \frac{n(0)}{N_0} = \frac{\pi^{1/2}}{2h(1 + N_c/N_{1/2})}, \quad (14a)$$

and

$$\beta_{\min} = \frac{\pi^{1/2}}{2h(2 + N_c/N_{1/2})}, \quad (14b)$$

where  $h$  is the effective height of the disk. The ratio  $\beta_{\max}/\beta_{\min}$  is always smaller than 2 and, given that the remnant is continuously decelerating, the weighted mean value of  $\beta$  over the evolution below the  $z = 0$  plane is close to  $\beta_{\min}$ . Therefore, a

simple and reliable approximation for the rest of the evolution can be obtained with

$$\beta \approx \frac{3 \times 10^{-21}}{2 + N_c/N_{1/2}} \text{ cm}^{-1}. \quad (15)$$

Thus, the remnant motion up to the maximum height,  $z_{\max}$ , is given by

$$\dot{z} = V_l = \exp[-\beta h \text{ erf}(z/H)] \times \left\{ V_0^2 - 2\alpha \int_0^z z \exp[2\beta h \text{ erf}(z/H)] dz \right\}^{1/2}, \quad (16)$$

and the solution to the equation of motion,  $z(t)$ , is obtained from

$$t = \int_0^z \frac{dz}{V_l}, \quad (17)$$

where  $z_{\max}$  and its corresponding time scale are defined by  $V_l = 0$ . After  $z = z_{\max}$  the remnant accelerates to fall back into the plane with a velocity

$$V_l = (2\alpha)^{1/2} \exp(-\beta h \gamma) \left[ \int_z^{z_{\max}} z \exp(2\beta h \gamma) dz \right]^{1/2}, \quad (18)$$

where  $\gamma = \text{erf}(z_{\max}/H) - \text{erf}(z/H)$ . The maximum velocity is achieved when the remnant reaches the plane again and the subsequent oscillatory motion is obtained with repeated applications of equations (16)–(18).

Figure 4 shows the motion after  $t_{GP}$  for the remnant shown in Figure 3b (i.e.,  $N_0 = 9 \times 10^{20} \text{ cm}^{-2}$  and  $V_0 = 30 \text{ km s}^{-1}$ ). The amplitudes,  $z_{\max}$  and  $V_l(z=0)$ , for successive oscillations are clearly reduced by the drag term but the oscillation periods,  $\sim 8 \times 10^7$  yr, do not differ much from the one corresponding to the simple harmonic oscillator (the difference is less than 10% for the case shown). The evolution is certainly sensitive to the value of the drag constant,  $\beta$ , and there are substantial differences in the evolution when  $\beta$  is increased or decreased by factors of about 3. Fortunately, as stated before, the ratio  $\beta_{\max}/\beta_{\min}$  is always smaller than 2 and the approximation introduced in equation (15) does not have an important effect on the final solution.

A simple and reliable expression for the evolution of the eccentricity is difficult to derive. Nevertheless, a rough, almost order of magnitude, estimate can be obtained with the isothermal shock approximation. Given the ambient sound speed,  $c$ , and the solution to  $V_l$  in equation (16), a lower bound to the central density in the remnant is given by

$$n_l \sim n(z) V_l^2 / c^2,$$

and, before self-gravity sets in, the eccentricity evolves approximately as

$$\epsilon \sim \left( 1 - \frac{e^{-2z^2/H^2} c^4}{4\beta^2 r_c^2 V_l^4} \right)^{1/2}.$$

#### iii) Tidal Forces

Self-gravitating clouds can be disrupted by galactic tidal forces if their size along the line joining the cloud center and galactic center is larger than a certain maximum radius,  $r_{\max}$ . The self-gravitational acceleration in the radial direction is given in equation (8a) and the tidal acceleration per unit distance is

$$F = \frac{2u^2}{R^2} - R^{-1} \frac{du^2}{dR}, \quad (19)$$

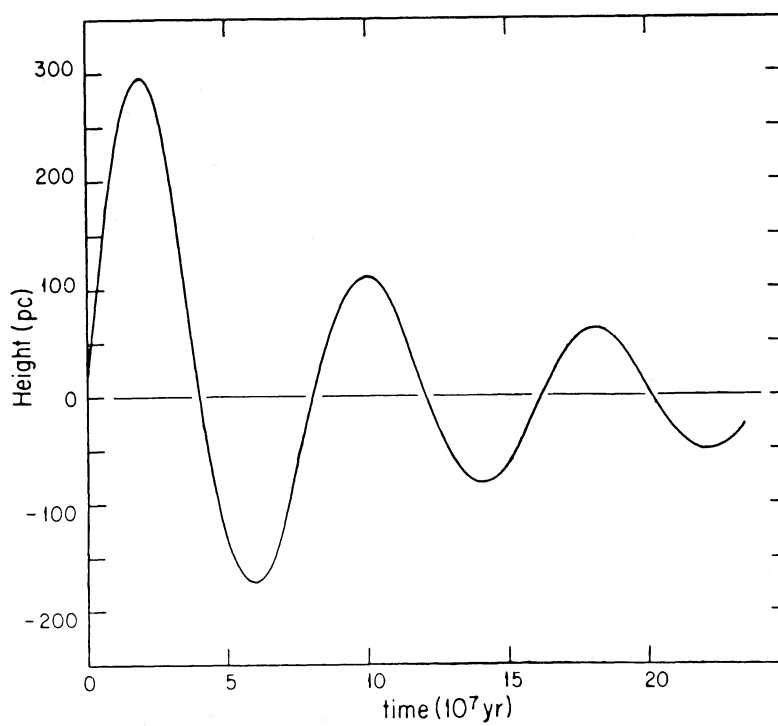
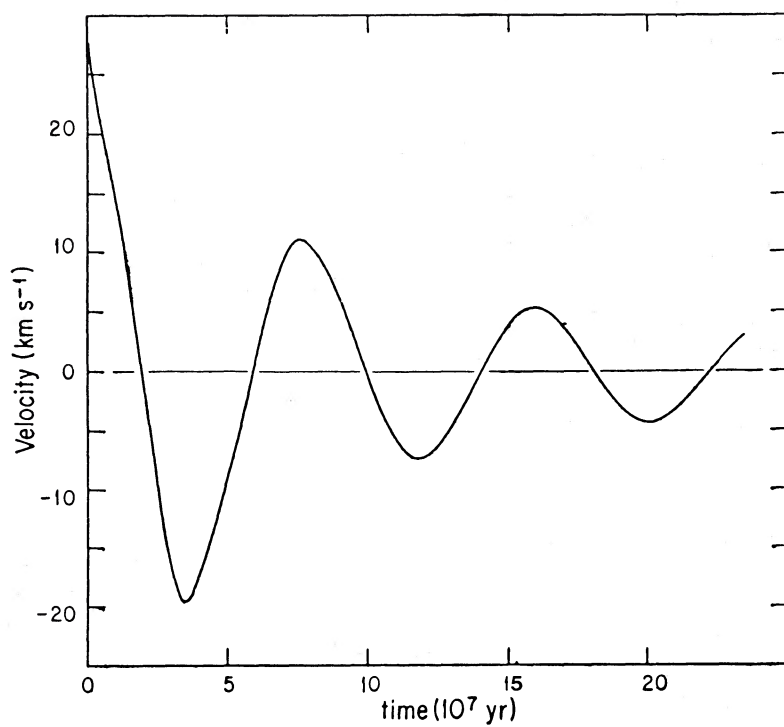


FIG. 4.—Solution to eq. (13) for the solar neighborhood with  $V_0 = 30 \text{ km s}^{-1}$  and  $\beta = 10^{-21} \text{ cm}^{-1}$

where  $u$  is the disk circular velocity, and  $R$  is the galactocentric distance. Stability against tidal disruption including internal pressure requires (see Stark and Blitz 1978)

$$\psi^2 + 2\psi^{-1} \geq 3 + A, \tag{20}$$

with

$$\psi = r_c/r_t, \tag{21a}$$

$$A = \frac{v^2}{Fr_t^2}, \tag{21b}$$

and

$$r_t = \mu\pi GN_1 f(\epsilon)/F, \tag{21c}$$

where  $v$  is the velocity dispersion inside the remnant. The tidal reference radius,  $r_t$ , corresponds to the zero pressure case and the maximum allowed radius,  $r_{\max}$ , is defined by the equal sign in equation (20). Assuming a flat rotation curve for the solar neighborhood with  $u_\odot = 225 \text{ km s}^{-1}$  and  $R_\odot = 8 \text{ kpc}$  (cf. Clemens 1985; Allen and Martos 1986), the tidal acceleration per unit distance in the solar circle is  $F_\odot = 1.8 \times 10^{-30} \text{ s}^{-2}$ , and the corresponding tidal reference radius is  $r_t = 90f(\epsilon)N_{21} \text{ pc}$  (where  $N_{21} = N_l/10^{21} \text{ cm}^{-2}$ ).

Figure 5 shows  $r_{\max}/r_t$  as a function of the internal pressure parameter  $A$ . In the case of the collision described in Figure 3b, with a collected column density  $N_l = 1.5 \times 10^{21} \text{ cm}^{-2}$  and a radius of about  $r_c = 200 \text{ pc}$ , the maximum radius allowed by tidal forces and internal pressure (assuming  $T = 10^3 \text{ K}$ ) is only  $r_{\max} \sim r_c/2 \sim 90 \text{ pc}$ . The size of this large remnant, then, is limited by tidal forces and it does not proceed as a single entity

through the whole evolution. Instead it is disrupted into at least two pieces on a time scale  $F^{-1/2}$  after the original HVC was shocked.

The fragmentation process operates during the whole evolution after  $t_{\text{ref}}$ , but the remnant collects interstellar matter in a time scale shorter than  $F_\odot^{-1/2} \approx 2.5 \times 10^7 \text{ yr}$  and it becomes self-gravitating before the fragmentation is completed. The resulting fragments, having the same column density as the parental remnant, are self-gravitating and stable against tidal disruption.

IV. THE CASE OF ORION AND MONOCEROS CLOUD COMPLEXES

a) The Collision

Within the scheme discussed in the previous section, the origin of the Orion and Monoceros complexes can be explained with a collision similar to the one shown in Figure 3b. A cylindrical HVC with  $N_c = 3 \times 10^{20} \text{ cm}^{-2}$ ,  $V_c = 100 \text{ km s}^{-1}$ , and  $r_c = 200 \text{ pc}$  approaching the solar neighborhood from the *southern galactic hemisphere* (see § IVb), generates a large-scale and massive shocked layer as it collides with the gaseous disk. The collision ends when the shocked layer is located at  $z_{\text{ref}} \approx 100 \text{ pc}$  (eq. [3]).

The resulting remnant reaches the galactic plane, some  $\sim 2 \times 10^6 \text{ yr}$  after  $t_{\text{ref}}$  (eq. [6]), with a radius similar to  $r_c$  and  $N_0 = 9 \times 10^{20} \text{ cm}^{-2}$ ,  $V_0 \approx 30 \text{ km s}^{-1}$ , and  $M_0 \approx 10^6 M_\odot$  (eq. [5] evaluated at  $t = t_{\text{GP}}$ ). After crossing the plane the shocked gas expands and decelerates rapidly because of the reversal of the galactic gravitational field. The massive remnant becomes molecular and self-gravitating (with  $N_l = 1.5 \times 10^{21} \text{ cm}^{-2}$ ) at

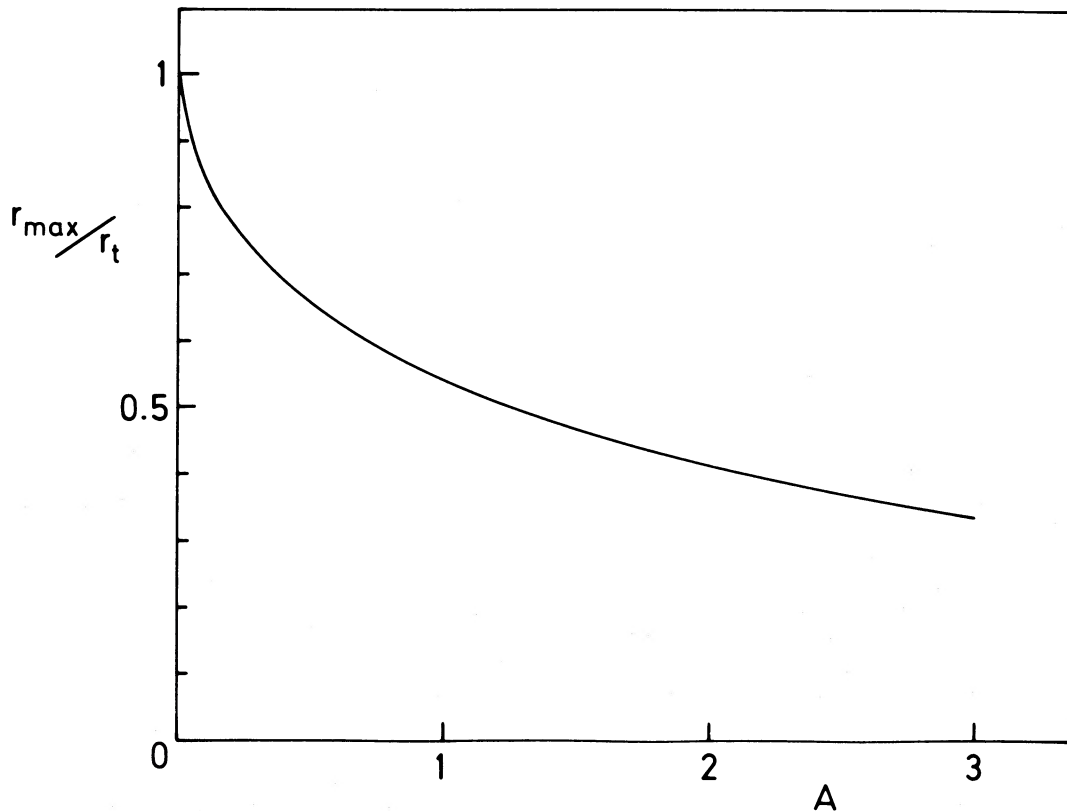


FIG. 5.—Maximum radius of a tidally stable cylindrical cloud  $r_{\max}$  (in units of the tidal reference radius  $r_t$ ) as a function of the internal pressure parameter  $A$ . The circle indicates the value for the evolution shown in Fig. 3b.

1988ApJ...333...826F

a height of about 150 pc after crossing the galactic plane (eqs. [10]–[12b]), some  $1.2 \times 10^7$  yr after  $t_{\text{ref}}$ , when its total mass amounts to  $\sim 2 \times 10^6 M_{\odot}$ . Tidal forces distort the remnant during the evolution, however, and induce its fragmentation on a time scale  $F^{-1/2} \sim 2.5 \times 10^7$  yr after  $t_{\text{ref}}$ .

This fragmentation process allows for a common origin of the two complexes. The maximum tidally stable radius is  $r_{\text{max}} \approx 90$  pc (eqs. [20]–[21c] with  $A = 0.6$ ), which is about a half of the actual remnant radius, and we assume that the remnant generates two stable cylindrical fragments, each with radius  $r_{\text{max}}$ , a mass  $M = \pi r_{\text{max}}^2 N_1 \mu \approx 4 \times 10^5 M_{\odot}$  (i.e., a total of about two-fifths of the parental remnant mass), and an initial separation of  $2r_{\text{max}} \sim 200$  pc. The projections of their centers of mass on the galactic plane are labeled by the galactocentric vectors  $\mathbf{R}_o$  and  $\mathbf{R}_m$  (with constant lengths  $R_o$  and  $R_m$ ; the subscripts o and m refer to the progenitors of the Orion and Monoceros complexes, respectively). Note that we are assuming that fragmentation is 50% efficient. If the rest of the remnant mass is locked in other self-gravitating pieces, their evolution is similar to the one described in this section. Otherwise the gas is simply dispersed. The structure of the Orion-Monoceros region is complicated enough that any of these alternatives is reasonable.

#### b) Fragment Separation due to Galactic Differential Rotation

Given that the solar circle is located at  $R_{\odot} = 8$  kpc, the actual galactocentric distance to the Orion complex is about 8.4 kpc. Setting  $R_o$  to this value, the corresponding length of  $R_m$  becomes 8.6 kpc (i.e., the center of the parental remnant was located at a galactocentric radius of 8.5 kpc) and the fragment separation as a function of time,  $\Delta_{o-m}(t)$ , is determined by their difference in orbital angular velocity about the galactic center,  $\theta_o = u_o/R_o$  and  $\theta_m = \mu_o/R_m$ .

Their distances to the Sun, which is assumed to be a point fixed on the galactic plane and defined by the vector  $\mathbf{R}_{\odot}$ , vary as

$$L_o(t) = [z(t)^2 + R_o^2 + R_{\odot}^2 - 2R_o R_{\odot} \cos(\tau_o)]^{1/2}, \quad (22a)$$

and

$$L_m(t) = [z(t)^2 + R_m^2 + R_{\odot}^2 - 2R_m R_{\odot} \cos(\tau_m)]^{1/2}, \quad (22b)$$

with

$$\tau_o = (\theta_o - \theta_{\odot})t + \delta, \quad (23a)$$

$$\tau_m = (\theta_m - \theta_{\odot})t + \delta, \quad (23b)$$

where  $z(t)$  is the height of the fragments at time  $t$ ,  $\theta_{\odot}$  is the angular velocity of the solar circle, and  $\delta$  is the angle between  $\mathbf{R}_{\odot}$  and both  $\mathbf{R}_o$  and  $\mathbf{R}_m$  at  $t = 0$ . Therefore, the relative distances are uniquely determined by the choice of the initial angle,  $\delta$ , and the time origin.

Given that the tidal distortion of the original remnant becomes important shortly after the passage of the plane, for simplicity we assume that the fragment separation begins at  $t_{GP}$  (but the fragmentation process is completed at  $F^{-1/2}$ , shortly before the first maximum height is reached). Then, at  $t = t_{GP} = 0$  the protofragments are situated on the plane and separated by  $\Delta_{o-m}(0) = 200$  pc. Their heights and  $z$ -velocities as a function of time, then, are given directly in Figure 4. It is clear from this figure that, under the assumption of a collision from the southern galactic hemisphere, the present locations of Orion and Monoceros, some 150 pc below the galactic plane, have only one solution at about  $t \approx 6 \times 10^7$  yr.

As shown in Figure 1, most of the projected HVCs are clustered in the southern galactic hemisphere. Nevertheless, if one assumes that the cloud came from the northern hemisphere, the present locations of these complexes require solutions in the neighborhood of  $2 \times 10^7$  yr or after one complete oscillation, at  $t \sim 10^8$  yr. The first solution is meaningless because it is smaller than the age of the older stars in Orion ( $\sim 3 \times 10^7$  yr; Isobe 1982, 1987). The second solution,  $t \sim 10^8$  yr, cannot be completely ruled out but, given the presence of massive stars in Orion, such an old age is difficult to justify.

Therefore, the best choice corresponds to an HVC approaching the solar neighborhood from the southern hemisphere, giving an evolutionary time scale of  $\sim 6 \times 10^7$  yr for the present moment and a present fragment separation of  $\Delta_{o-m}(6 \times 10^7 \text{ yr}) = 380$  pc, which is certainly consistent with the observed separation between Orion A and Mon R2 ( $\sim 400$  pc). The distances to both complexes from the Sun represent additional constraints for our model and they fix the appropriate value for  $\delta$ . Using the distance to Orion, 500 pc, as the main constraint, equation (22a) sets the initial angle to  $\delta \approx 3^\circ$  and this in turn yields a present distance to the other fragment of  $L_m(6 \times 10^7 \text{ yr}) \approx 850$  pc, which is in good agreement with the distance to Mon R2.

The final outcome of the model is summarized in Figure 6, which shows the evolution of the fragments as seen from the Sun. Their positions at  $t = 6 \times 10^7$  yr are in agreement with the actual locations of the main bodies of the Orion and Monoceros complexes, as seen in Figure 1.

#### V. DISCUSSION

One of the important open problems in interstellar physics is that of the formation of giant molecular clouds; numerous ideas have been put forward regarding this question. Often discussed in this connection is the Parker instability (Parker 1966) which, driven by a change in the magnetic pressure in the direction perpendicular to the galactic plane, can be triggered by the galactic spiral density wave (Mouschovias, Shu, and Woodward 1974). Another process is the gradual buildup of large clouds by the collisions of small clouds. A recent detailed numerical investigation by Lattanzio *et al.* (1985) shows that for most reasonable sets of parameters collisions of isothermal clouds result in dispersal of cloud material rather than agglomeration. Therefore, if the process is to work at all, it probably requires the density enhancement provided by spiral waves (cf. Kwan and Valdes 1983) or a magnetic linking of the structures (Elmegreen 1987).

Expanding supernova shells can also lead to conditions conducive to cloud formation and, even, self-regulated star formation (Franco and Shore 1984). The remnants caused by the sequential explosion of  $\sim 50$  supernovae in an OB association produce a column density in the swept-up shell that is sufficiently high to allow molecular formation and gravitational instability (Tenorio-Tagle and Palouš 1987; McCray and Kafatos 1987). A further possibility is gravitational instability on a galactic scale (Elmegreen 1979; Elmegreen and Elmegreen 1983). The instability can result in the collapse of H I clouds with masses  $\sim 10^7 M_{\odot}$ ; in this picture the molecular cloud complexes ( $\sim 10^5 M_{\odot}$ ) form in the cores of these large-scale structures.

The present paper proposes a new mechanism: compression and gravitational instability induced by the impact of a high-velocity cloud with the galactic disk. This mechanism is not suggested as a general formation process which can explain all

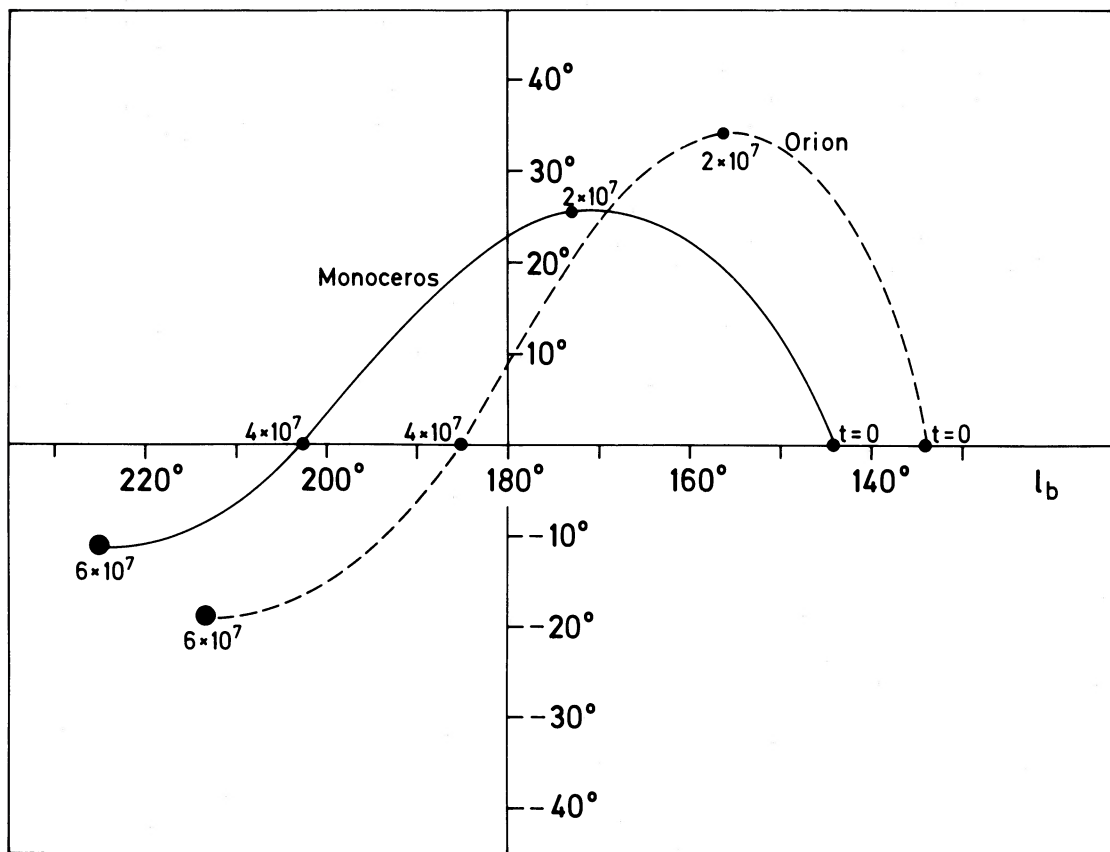


FIG. 6.—Evolution of the progenitors of the Orion and Monoceros complexes (see text) as seen from the Sun in galactic coordinates. Their positions at  $t = 0$  are defined by the position of the parental remnant at  $t_{\text{GR}}$ , and their present locations correspond to  $t = 6 \times 10^7$  yr.

types of molecular clouds. Rather, it is thought to apply in special cases, such as that of the Orion and Monoceros complexes which are located well below the galactic plane in comparison with most other molecular clouds.

The precise physical properties of the high-velocity H I clouds are difficult to determine observationally. Their H I column densities fall in the range  $2 \times 10^{18}$ – $10^{21}$   $\text{cm}^{-2}$ , most of them are moving toward the galactic plane with velocities up to  $200 \text{ km s}^{-1}$ , and at least some of them appear to originate from outside the Galaxy, in the Magellanic stream (Mirabel 1981a, b). Their distances can only be estimated in a rough manner. The resulting deduced sizes fall in the range 50–500 pc, their masses,  $10^4$ – $10^6 M_{\odot}$ , and their kinetic energies,  $5 \times 10^{51}$ – $3 \times 10^{53}$  ergs. Three requirements must be met if the collision of such a cloud with the galactic disk is to result in the formation of a molecular cloud. (a) The shocked layer produced as a result of the collision must maintain a column density  $N_l > 10^{21} \text{ cm}^{-2}$  for several million years in order to allow the formation of molecules. (b) The momentum of the original cloud must be above a certain critical value ( $2 \times 10^{20} \text{ cm}^{-2}$  at a velocity of  $100 \text{ km s}^{-1}$  for the solar neighborhood), so that the cloud will not have time to reexpand and disperse after the collision is completed, and the shocked layer is able to reach and penetrate somewhat beyond the galactic plane. (c) The column density of the cloud plus that of the swept-up galactic matter must exceed the critical value required for gravitational instability. The numerical calculation presented here shows that all conditions can be met, for galactic disk properties characteristic of the solar neighborhood, if one assumes a

cylindrical cloud with the following initial properties: density  $1 \text{ cm}^{-3}$ , velocity  $100 \text{ km s}^{-1}$ , height 100 pc, radius 200 pc, mass  $3 \times 10^5 M_{\odot}$ , and kinetic energy  $3 \times 10^{52}$  ergs. Clouds with other parameters, of course, may also achieve the desired results, but the range of allowable parameters has not been explored here. Note, however, that outside the solar circle, say at 20 kpc from the galactic center, the required conditions would not be met because of the lower column density in the disk. The expected result of the collision would be the production of a large-scale expanding shell (Paper II; Kulkarni and Mathieu 1986), rather than a molecular cloud.

The particular case which fits the observed properties of Orion and Monoceros has been examined in detail. The infalling cloud is assumed to have a velocity in the  $z$ -direction with respect to the Galaxy; components parallel to the galactic plane are neglected. In general we would expect that the angular momentum of the infalling material with respect to the Galaxy would be nonnegligible unless the cloud originated from a “galactic fountain” (Bregman 1980). The main effects of an azimuthal component in the cloud velocity are: (a) there is a drift of the remnant in a direction parallel to the disk (which is continuously reduced by the interstellar drag), and (b) the mass collected by the drift increases the column density of the main shock at a given height from the plane. Therefore, the high-opacity column density may be reached earlier than the time given in our calculations. However the general case is difficult to model because it requires three-dimensional hydrodynamics.

The numerical calculation is carried up to the point where

all of the above criteria are satisfied; the shocked layer would then begin to contract under the influence of its own gravity. The numerical code does not include self-gravity, nor does it include magnetic fields, which of course would tend to support the cloud against collapse. Galactic tidal forces are then assumed to result in fragmentation of the object into two equal parts of  $5 \times 10^5 M_{\odot}$  each, and initially separated by 200 pc. The time scale of action of the tidal force is estimated to be  $2.5 \times 10^7$  yr, which is close to the time required for the layer to reach the self-gravitating stage ( $1.2 \times 10^7$  yr) and about equal to the time required for the layer to reach its maximum height beyond the galactic plane. For simplicity the fragmentation is assumed to begin at the moment of passage through the plane, and the fragment centers are assumed to lie in the same direction as viewed from the galactic center. A full three-dimensional numerical calculation is required for the actual determination of these quantities. If fragmentation actually occurs at a different time or the orientation of the centers is different, a solution is still possible with some changes in the initial cloud parameters; this question, however, has not been investigated in detail.

The subsequent motion of the fragments is simply estimated by the solution of the equation of motion of point masses in the gravitational potential of the differentially rotating galaxy. The model explains the position and masses of both the Orion and Monoceros complexes after the reasonable time of  $6 \times 10^7$  yr after the fragmentation begins. The fit occurs near the time of maximum amplitude after the second passage through the galactic plane; the  $z$ -motion of these objects and the stars that were formed by them would therefore be expected to be very small (below  $5 \text{ km s}^{-1}$ ). The present radii of the Orion A and Mon R2 clouds (50 pc) are somewhat smaller than the original fragment radii (100 pc) but some contraction is expected on the fragment free-fall time ( $\sim 10^7$  yr). The model is consistent with the probable age of the Orion complex. If it turns out that the Monoceros complex is significantly younger, then the model

would have to be modified; it is of course possible to explain the origin of the two complexes by separate impacts of independent high-velocity clouds. An observational test for their common origin would be the detection of a connecting bridge of interstellar matter, as already suggested by Maddalena *et al.* (1984).

Finally, this model is not intended to explain at the same time the formation or expansion energy of the Gould belt. Nonetheless, the possible association of Orion to the belt as well as the estimated age of the belt indicate that this same collision was also responsible for the observed tilt. As discussed in § IIc, there are other distortions or random perturbations in the galactic disk, and one may ask whether HVC interactions may be responsible for all of them. At the present time it would be premature to draw any firm conclusions, because the mass accretion rate of high-velocity material is unknown. In line with our previous conclusion regarding the formation of molecular clouds, we suspect that such a connection can be made only in particular cases.

We thank J. Galindo and J. F. Barral for useful hints in dealing with the solution of equation (13). P. B. thanks the Alexander von Humboldt Foundation for a US Senior Scientist Award. He was also supported in part under the auspices of a special NASA astrophysics theory program which supports a joint Center for Star Formation Studies at NASA-Ames Research Center, U. C. Berkeley, and U. C. Santa Cruz. J. F. thanks the Max-Planck-Institut für Astrophysik, Garching, and CONACyT-México for partial financial support. I. F. M. is a member of CONICET-Argentina and acknowledges partial support from the NSF-Epscor program at Puerto Rico. M. R. acknowledges the hospitality and financial support provided by the Max-Planck-Institut für Astrophysik, Garching. G. T.-T. is supported by the Deutsche Forschungsgemeinschaft grant MO416, and thanks the DAAD-Germany and CONACyT-México for travel grants.

## REFERENCES

- Allen, C., and Martos, M. A. 1986, *Rev. Mex. Astr. Astrofis.*, **13**, 137.  
 Avedisova, V. S., and Palouš, J. 1988, *Bull. Astr. Inst. Czech.*, in press.  
 Blaauw, A. 1964, *Ann. Rev. Astr. Ap.*, **2**, 213.  
 Bregman, J. N. 1980, *Ap. J.*, **236**, 577.  
 Clemens, D. P. 1985, *Ap. J.*, **295**, 422.  
 Elmegreen, B. G. 1979, *Ap. J.*, **231**, 372.  
 ———, 1987, in *Physical Processes in Interstellar Clouds*, ed. G. E. Morfill and M. Scholer (Dordrecht: Reidel), p. 1.  
 Elmegreen, B. G., and Elmegreen, D. M. 1978, *Ap. J.*, **220**, 1051.  
 ———, 1983, *M.N.R.A.S.*, **203**, 31.  
 Franco, J. 1986, *Rev. Mex. Astr. Astrofis.*, **12**, 287.  
 Franco, J., and Cox, D. P. 1986, *P.A.S.P.*, **98**, 1076.  
 Franco, J., and Shore, S. N. 1984, *Ap. J.*, **285**, 813.  
 Frogel, J. A., and Stothers, R. 1977, *A.J.*, **82**, 890.  
 Gerola, H., and Glassgold, A. E. 1978, *Ap. J. Suppl.*, **37**, 1.  
 Heiles, C. 1984, *Ap. J. Suppl.*, **55**, 585.  
 Heiles, C., and Jenkins, E. B. 1976, *Astr. Ap.*, **46**, 333.  
 Hirth, W., Mebold, U., and Müller, P. 1985, *Astr. Ap.*, **153**, 249.  
 Hughes, V. A., and Baines, J. G. N. 1985, *Ap. J.*, **289**, 238.  
 Isobe, S. 1982, *Ann. N. Y. Acad. Sci.*, **395**, 65.  
 ———, 1987, *Ap. Space Sci.*, **135**, 237.  
 Kalberla, P. W. M., Herbstmeier, U., and Mebold, U. 1984, in *IAU Colloquium 81, Local Interstellar Medium*, ed. Y. Kondo, F. C. Bruhweiler and B. D. Savage (NASA-CP2345), p. 243.  
 Kraushaar, W. L. 1979, in *X-Ray Astronomy (COSPAR)*, ed. W. A. Baity and L. E. Peterson (New York: Pergamon), p. 293.  
 Kulkarni, S., and Fich, M. 1985, *Ap. J.*, **289**, 782.  
 Kulkarni, S., and Mathieu, R. 1986, *Ap. Space Sci.*, **118**, 531.  
 Kwan, J., and Valdes, F. 1983, *Ap. J.*, **271**, 604.  
 Lattanzio, J. C., Monaghan, J. J., Pongracic, H., and Schwarz, M. P. 1985, *M.N.R.A.S.*, **215**, 125.  
 Lesh, J. R. 1968, *Ap. J. Suppl.*, **17**, 371.  
 Maddalena, R. J., Morris, M., Moscowitz, J., and Thaddeus, P. 1986, *Ap. J.*, **303**, 375.  
 McCray, R., and Kafatos, M. 1987, *Ap. J.*, **317**, 190.  
 McKee, C. F., and Hollenbach, D. J. 1980, *Ann. Rev. Astr. Ap.*, **18**, 219.  
 Mestel, L. 1965, *Quart. J.R.A.S.*, **6**, 161.  
 ———, 1966, *M.N.R.A.S.*, **131**, 307.  
 Mirabel, I. F. 1981a, *Rev. Mex. Astr. Astrofis.*, **6**, 245.  
 ———, 1981b, *Ap. J.*, **247**, 97.  
 ———, 1982, *Ap. J.*, **256**, 112.  
 Mouschovias, T., Shu, F., and Woodward, P. 1974, *Astr. Ap.*, **33**, 73.  
 Nyman, L., Bronfman, L., Cohen, R., and Thaddeus, P. 1987, *Ap. J.*, **314**, 374.  
 Olano, C. A. 1982, *Astr. Ap.*, **112**, 195.  
 Parker, E. E. 1966, *Ap. J.*, **145**, 811.  
 Reynolds, R. J., and Ogden, P. M. 1979, *Ap. J.*, **229**, 942.  
 Sanders, D. B., Solomon, P. M., and Scoville, N. Z. 1984, *Ap. J.*, **276**, 182.  
 Spitzer, L., Jr. 1978, *Physical Processes in the Interstellar Medium* (New York: Wiley).  
 Stark, A. A., and Blitz, L. 1978, *Ap. J. (Letters)*, **225**, L15.  
 Stark, A. A., and Brand, J. 1988, preprint.  
 Stothers, R., and Frogel, J. A. 1974, *A.J.*, **79**, 456.

Tarafdar, S. P., Prasad, S. S., Huntress, W. T., Jr., Villere, K. R., and Black, D. C. 1985, *Ap. J.*, **289**, 220.  
 Taylor, D. K., Dickman, R. L., and Scoville, N. Z. 1987, *Ap. J.*, **315**, 104.  
 Tenorio-Tagle, G., Bodenheimer, P., Różyczka, M., and Franco, J. 1986, *Astr. Ap.*, **170**, 107 (Paper I).

Tenorio-Tagle, G., Franco, J., Bodenheimer, P., and Różyczka, M. 1987, *Astr. Ap.*, **179**, 219 (Paper II).  
 Tenorio-Tagle, G., and Palouš, J. 1987, *Astr. Ap.*, **186**, 287.  
 Thaddeus, P. 1982, *Ann. N.Y. Acad. Sci.*, **395**, 9.  
 van der Hulst, T., and Sancisi, R. 1988, *A.J.*, **95**, 1354.

P. BODENHEIMER: Lick Observatory, University of California, Santa Cruz, CA 95064

J. FRANCO: Instituto de Astronomía-UNAM, Apdo. Postal 70-264, 04510 México D. F., México

I. F. MIRABEL: Instituto de Astron. y Fis. del Espacio, Casilla de Correo 67, Suc. 28, Buenos Aires, Argentina

M. RÓŻYCZKA: Warsaw University Observatory, Al. Ujazdowskie 4, 00478 Warszawa, Poland

G. TENORIO-TAGLE: Max-Planck-Institut für Astrophysik, D-8046 Garching bei München, Federal Republic of Germany